

Growth and corrosion behaviors of thin anodic alumina membrane on AA5083 Al–Mg alloy in incandescent medium

Jia-yu WANG, Cheng LI, Shun-li ZHENG, Cheng-yong YIN, Yan-hui WANG

College of Materials Science and Technology, Nanjing University of Aeronautics and Astronautics,
Nanjing 210016, China

Received 29 August 2013; accepted 3 December 2013

Abstract: A self-ordered porous film was fabricated on aluminum alloy in a ternary boric–sulfuric–oxalic acid electrolyte system. By means of voltage–time response, the oxidation process as well as the growth efficiency was studied. Field emission scanning electron microscopy (FE-SEM) was adopted to reveal the morphological and microstructural features of as-fabricated oxide layers. The corrosion protection properties of the films were investigated by electrochemical impedance spectroscopy and potentiodynamic polarization measurements. The results showed that increasing the concentration of the double ionic layer located at the oxide interface could accelerate the film growth rate. The anodic oxidative layer with thickness of 8–9 μm and pore diameter of 10–14 nm maintains the pattern and topography of workpieces, compared with the overall closed film with hierarchical structure. Both samples exhibited much lower corrosion current density after boil water sealing. Meanwhile, a superior stability could be achieved through raising the ambient temperature.

Key words: 5083 aluminum alloy; anodizing; film growth efficiency; corrosion behavior

1 Introduction

Compact alumina oxide layer formed by anodizing processes, with a self-ordered porous structure on aluminum alloys, can improve the optimized characteristics of the surface and enhance the corrosion resistance of workpiece [1]. The formation of anodic aluminum oxide (AA) film includes two parts. For one part, several acids and mixtures [2] are practically applied for traditional anodizing processes, such as sulfuric acid, phosphoric acid and chromic acid. For another part, various factors have also been taken into account in preparing porous film on aluminum alloy parts, such as temperature of electrolyte [3], shape of workpieces [4], anodizing step process [5], technical parameters [6,7] and sealing methods [8,9]. The growth of the oxide film on matrix is affected by both of these two parts leading to a decreased anti-corrosion behavior of appliance [10,11].

The boric–sulfuric acid anodizing process (BSA) has drawn more and more attention in surface morphology and corrosion resistance as it is an alternative to traditional chromic acid anodizing [12]. Examination of oxide films formed by BSA process has

generally revealed that the fatigue resistance of the anodized specimens is satisfactory to practical applications and these properties are not significantly different from those of chromic acid anodizing [13]. However, porous layer always results in variations in the protective performance in chloride-containing medium [14]. Consequently, the durability of AA films could be destroyed by penetration of aggressive agents, especially when working in an atrocious surrounding with uncertainty temperatures [15].

In this work, three boric–sulfuric–(oxalic) acid electrolytes were applied to preparing anodic alumina film on 5083 aluminum alloy. The aim of two thermal/hydration methods for AA films using hot air and boiling water is to investigate possible mechanism of pore growth, morphology of oxide layer, and electrochemical behaviour in temperature-controlled corrosion medium of 10–60 °C.

2 Experimental

Specimens prepared from the middle of an extruded T-shaped beam of aluminum alloy 5083 with following composition (mass fraction): 0.08% Cu, 0.13% Cr, 0.03% Ti, 4.9% Mg, 0.5% Mn, 0.3% Fe, and balance Al,

were mechanically ground with 800, 1200 and 4000 grit silicon carbide paper. For cleaning the surface, the electrodes were etched with a 5% solution of NaOH at room temperature and rinsed in a 50% (volume fraction) HNO₃ solution, and then immersed in a brightening solution (85% H₃PO₄, 16% H₂SO₄, 3% HNO₃, volume fraction) at 20–25 °C for 1–3 min, and rinsed with distilled water.

The anodisation of these specimens was carried out in a two-electrode cell with instruments: a regulated DC power supply, an electrolyte bath and a cooling device. The anodising process was immersed in boric–sulfuric–oxalic acid (BS: H₂SO₄ 0.51 mol/L, H₃BO₃ 0.097 mol/L; BSO-1: H₂SO₄ 0.51 mol/L, H₃BO₃ 0.097 mol/L, C₆H₈O₇ 0.067 mol/L; BSO-2: H₂SO₄ 0.51 mol/L, H₃BO₃ 0.097 mol/L, C₆H₈O₇ 0.111 mol/L) and held for 40 min (20 °C). After the anodizing process, the formed alumina layer was then divided into three parallel plates without any cracks on the surface. The first sample was dried at 40 °C in air (IAA); the second sample was heat treated in hot air (100 °C) for 30 min (AAA); the third sample was rinsed with boiling water for 30 min and then dried in hot air (BAA). Three plates showed a perceptible distinction from light grey to fuzzy white.

The microstructure of AA film was examined by a field emission scanning electron microscope (FESEM, Hitachi S–4800, Tokyo) in high vacuum, with an acceleration voltage of 10.0 kV. The thickness of resulting AA film was measured using a Minitest thickness detector supported by a 600 F/N probe (Elektrophysik, Model FN2, Hamburg) and revised 10 times. All electrochemical tests were recorded by using an electrochemical workstation (CHI 750C, Shanghai) connected to a conventional three-electrode cell system with a saturated calomel electrode (SCE) as reference electrode and a platinum plate as auxiliary electrode, and the working electrode prepared by edge-banding anodic sheet with effective surface of 10 mm×10 mm. Prior to electrochemical impedance spectroscopy (EIS) and potentiodynamic polarization measurements, immersion for 1500 s was given to the aforementioned solution to reach a stable state during open-circuit potential measurements. For EIS measurements, a sinusoidal AC perturbation of 5 mV amplitude was applied to the electrode at its open circuit potential over the frequency range of 10 mHz to 100 kHz. Polarization experiment was performed with a scan rate of 5 mV/s, and all samples were tested at least three times within 300 mV based on the steady open circuit potential.

3 Results and discussion

3.1 Film formation efficiency for boric-sulfuric-oxalic acid anodization

For porous film growth, the outward transport of

Al³⁺ cations that form the new film material at the metal/oxide interface accounts for about 60% of the ionic current through the porous layer with the inward migration of O²⁻ ions. About 40% cations located at the metal/oxide interface migrate further under the electric field with eventual ejection into the electrolyte. So the formation efficiency is commonly known as about 60%.

In order to estimate the formation efficiency (η) of the AAO film formed in BSO acid electrolyte, anodizing operations were performed in three BSO acid solutions with different current densities. The calculated formula for η could be expressed as [16]

$$\eta = \frac{m_2 - m_1 + [ItA/(3en)]}{[ItB/(6en)]}$$

where m_1 and m_2 are the specimen mass before and after anodization, respectively; I is the applied current; t stands for anodizing time; e is the electric quality of electron (1.6×10^{-19} C); n is Avogadro's constant (6.02×10^{23}); A is the relative atomic mass of Al and B is the relative molecular mass of Al₂O₃.

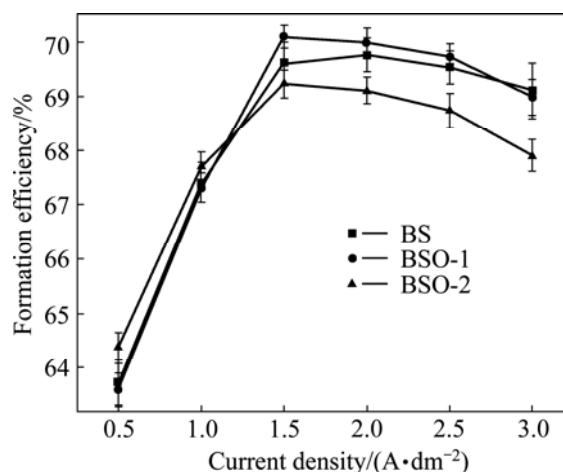


Fig. 1 Film formation efficiency against current density in three acid electrolytes

The results represent that the evolutions of the formation efficiency against current density in three BSO acid electrolytes all follow a schematic quadratic equation. In the range of 0.5–3 A/dm², the formation efficiency decreases with increasing electrolyte concentration, and almost remains constant when the current density does not exceed 1.5 A/dm². It can be seen that the calculated value in BSO-1 acid solution at 1.5 A/dm² takes up about 70.1%. Organic additive may induce notable viscosity at film/electrolyte interface. Therefore, the gradual increase of formation efficiency in BSO-1 electrolyte may be related with the resultant increase of the interface concentration. This is because that the dispersion of those produced ions may be more difficult for the rise of electrolyte viscosity.

3.2 Conditions for porous film growth

The classical voltage and current curves against time are recorded in Fig. 2. Sequential anodizing treatments are carried out at 1.5 A/dm^2 with a calculated rate of 2.5 V/min . Multiple-step stage procedures are used: 1) voltage of 2.5 V firstly raised in 30 s from marked minutes, followed by holding for later 30 s ; 2) the corresponding current firstly represents a rapid jump due to the gradual increase of anodizing voltage, followed by a recovery with the stable voltage, and finally a little increase of the current. From a schematic view of the stages during voltage increase ($\Delta V=2.5 \text{ V}$), at the first stage, the pre-formed Al_2O_3 produced in a mixed electrolyte is present. The rise of voltage could promote electric field above the critical electric field which enhances the dissolution rate of the oxide and leads to disordered pores with relatively small spacings [7]. The single rise-descend-rise vibration of the current transient reveals furthermore a new ionic equilibrium, which is formed between film/electrolyte corresponding to voltage. From the reappearance of this step, it can be concluded that the stability of the oxide formed during voltage increase with the increasing concentration of ionic in film/electrolyte. The final voltage can be about 25 V and then kept for 0.5 h . The instantaneous temperature of electrolyte during the growth of the anodic films tends to increase at $20\text{--}31 \text{ }^\circ\text{C}$. Such an increase of temperature on the sample surface and the electrolyte results in a downwards of the anodizing voltage at the end (23.5 V).

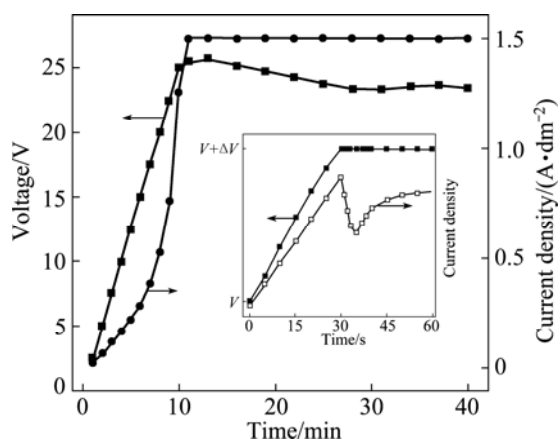


Fig. 2 Anodizing procedure at 1.5 A/dm^2 in BSO-1 electrolyte and schematic view of stages during voltage increase ($\Delta V=2.5 \text{ V}$)

It should be noted that with the linear increase of voltage, the current follows a non-linear curving trajectory. The anodic film/alloy interface is located from the first 6 min below 15 V , which coincides with the growth of the high density pore-free barrier (Fig. 3(a)) and increase of resistance; however, the signal for linear

increase was superimposed at about 20 V during the anodizing process, and then expanded to porous Al_2O_3 film (Fig. 3(b)). The flat film/electrolyte interface is unstable in response to local perturbations of electron and mass transfer. The sites of the initial pores depend upon the topography of the original aluminum surface, while the size of the resulting pore depends upon the electrolyte and voltage during the anodizing process (Fig. 3(c)). Some incipient pores stop growing and form the innermost layer, while others develop into the major structure of the porous film. The pore diameter, up to a few nanometers, depends on and increases with the limited temperature and H^+ activity at pore bases.

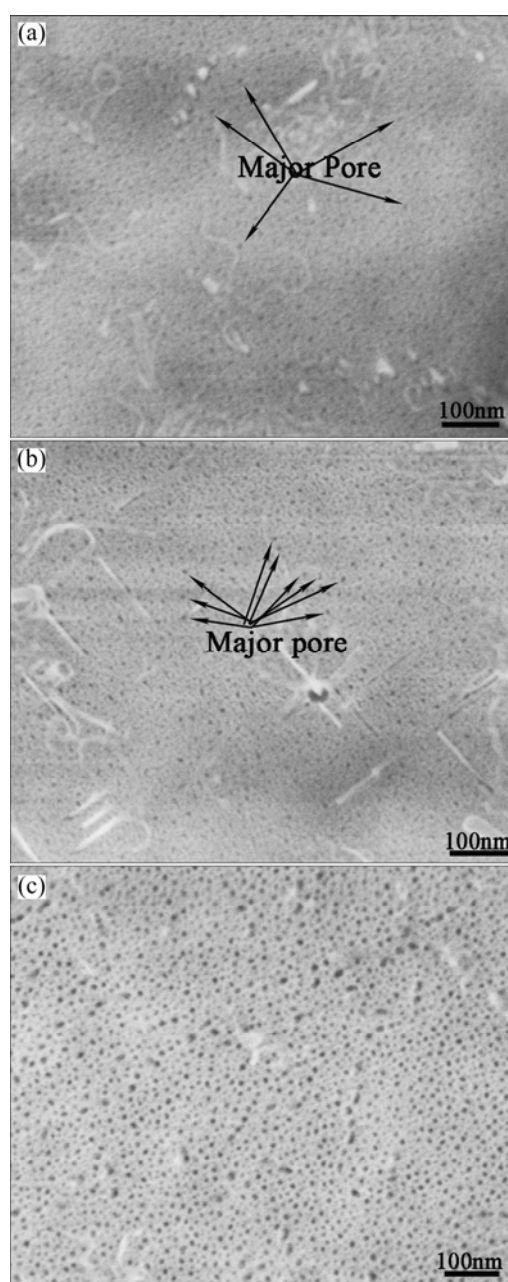


Fig. 3 FESEM images of extended pores in AA layer after anodization at selected voltage: (a) 15 V ; (b) 20 V ; (c) 23.5 V

An eddy current thickness test formed in different procedures resulted in an invisible increase of thickness, equivalent to 8–9 μm for porous film and 9.5 μm for BAA film.

3.3 Morphology of oxide layer

As shown in Fig. 3(c), for BSO acid electrolyte in this work, both the pores of IAA and AAA films are usually well ordered and uniform with diameter ranging from 10 to 14 nm which are made by measuring pores of top layer (Fig. 4(a)). The anodic alumina surface sealed in hot air (Fig. 4(b)), on which universal and well schemed pores spread, shows relatively flat and only several grain boundaries visible. For films dried at 40 $^{\circ}\text{C}$ in air (IAA), the configuration of surface in the films is similar, corresponding to diameter of 10–14 nm; however, disparity between bright regions and dark regions indicates the presence of residual hydrates in the film (Fig. 4(a)). After blocking process in boiling water (Figs. 4(c) and (d)), the entire surface consists of thin curved platelets with orientations nearly perpendicular to the substrate.

The surface of IAA and AAA film means a possible evaluation for mechanism of this structure transition, whereas that of BAA film has a distinct change (Fig. 4(c)). In hot air sealing procedure, only a little

change is caused by the escape of water during the air-sealing process. As comparison, the sealing measurement in boiling water will close most of the opening pores through partial conversion of anhydrous Al_2O_3 into $\text{Al}_2\text{O}_3\cdot\text{H}_2\text{O}$, in which water is an important participant of the reaction. For the direct cell wall between two neighbor pores, the oxide could be dissolved and transferred into sealed media under the driving effect of the cavitation. As a result, pore size of the film tends to be constricting, and then the top layer of the AA film is eventually plugged. The overall process involves a complex mechanism which consists of a series of stages (Fig. 4(d)) that lead to forming total layers with different strata: an outer layer of boehmite crystals, an intermediate and thicker layer which keeps a porous cell structure, and an innermost layer. The innermost layer, approach to matrix, is extremely thin and pore-free. The special surface structure of BAA sample promotes more areas for conglutination between the AA film and functional coating than the IAA and AAA films.

Lengthwise pores open towards the surface due to the chemical and electro-assisted dissolution of oxides during anodizing process. However, sealing process leads to a flake-like oxide structure due to random dissolution of pore walls by the boiling water. It should be noted that the length of thin curved platelets is quite

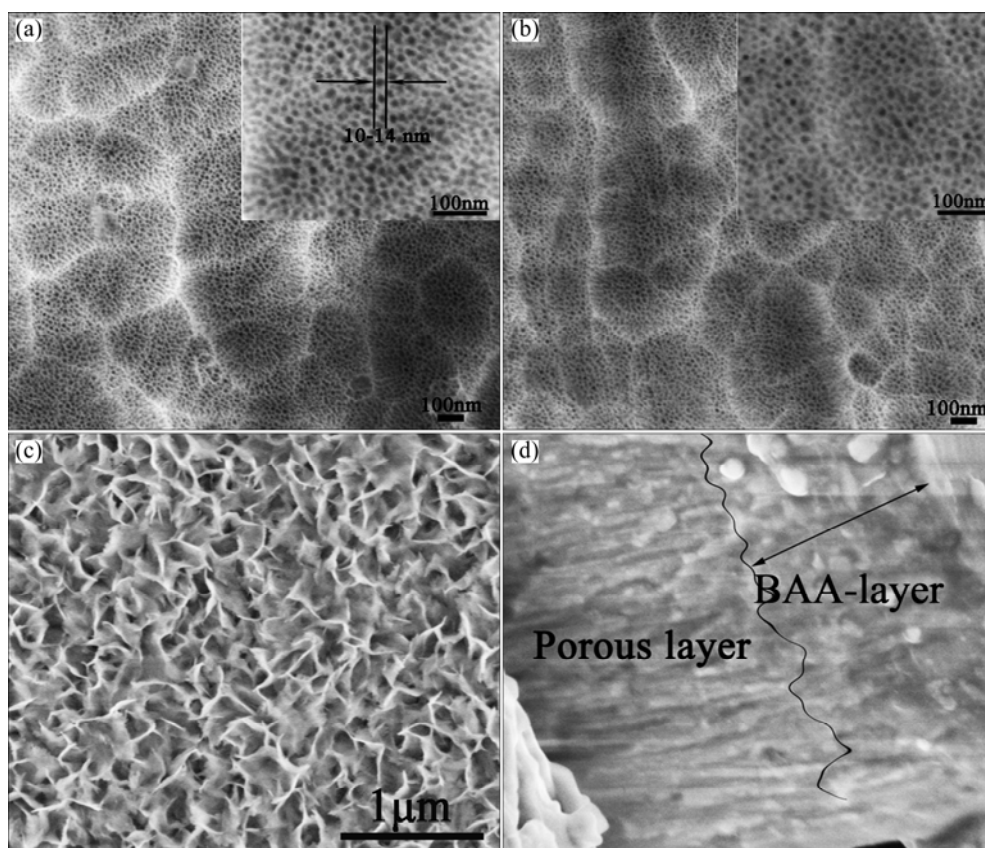


Fig. 4 SEM images of porous structure of IAA (a) and AAA (b) film, total sealed surface of BAA film (c), cross-section of BAA film (d) on 5083 aluminium alloy

larger than cell wall among neighbored pores. This originated dissolving behavior indicates that well structured framework encapsulated parallel pores have been formed, which could ensure good dispersion of pores and structural support of membrane on matrix. The sealed morphology observed in the absence or presence of pore is roughly similar to a hexagonal matrix.

3.4 EIS spectra and EC models

The typical impedance diagrams of samples with IAA, AAA or BAA film are shown in Fig. 5(a). It can be seen that the impedance for AAA sample represents little higher than that for IAA in all frequencies, whereas, the impedance for BAA sample differs in a wide frequency range, by 2–3 orders of magnitude higher than that of AAA and IAA samples. The increase of impedance exhibits an improvement of the protective oxide film after sealing process. The maximum experimental phase angles for the samples with IAA or AAA film were 90° associated with intermediate frequencies between 1 Hz and 10^3 Hz, which indicates the nature of the electric double layer formation. At intermediate and lower frequencies, the Bode magnitude displayed a linear slope of about -1 , indicating a typical capacitive behavior.

The electrochemical behaviors of samples with IAA, AAA and BAA films are different and the difference can

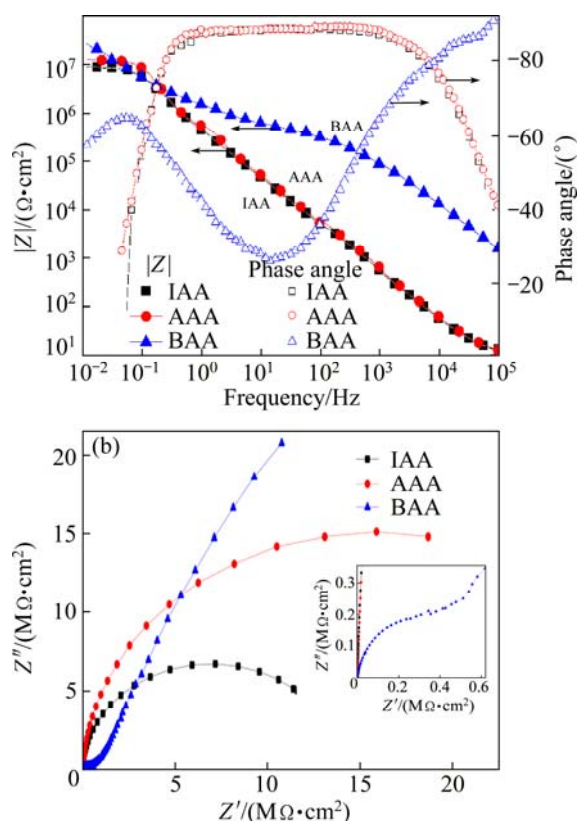


Fig. 5 Nyquist (a) and Bode (b) curves of workpieces with IAA, AAA or BAA film in 3.5% NaCl solution

be clearly seen on the Nyquist curves (Fig. 5(b)). The diameters of the plots of the samples with porous layer increase with the sealing measurement, indicating an increase in the oxide film resistance. Samples with IAA or AAA films represent only one semicircle. In contrast, for the films sealed in boiling water, small depressed semicircles were observed at high frequency, followed by the second larger semicircles at lower frequency. The first semicircle corresponds to the frequency range where the impedance depends on charge transfer, indicative of infiltration of the film.

To rebuild the existing possible mechanism of multiple anodic films, several optional simulations were analyzed. Further studies on hierarchical structure are also summarized in Fig. 6 and Table 1. The equivalent circuit for the samples with unsealed and air-sealed AA film (Fig. 6(a)) fitted to the experimental data contains the solution resistance R_s , the porous film resistance R_t and the constant-phase element CPE_{dl} for the porous film. Charge transfer resistance is caused by the redox reaction barrier on electrode when it is in contact with the electrolyte. An effectively protective AA film should bring up a value of this resistance. The more significant performance of the sample that is evident as corrosion resistance in the alumina film is probably due to an increasing charge transfer resistance, which has been shown by high impedance value of AAA film obtained and confirmed the function of a hot air-seal process.

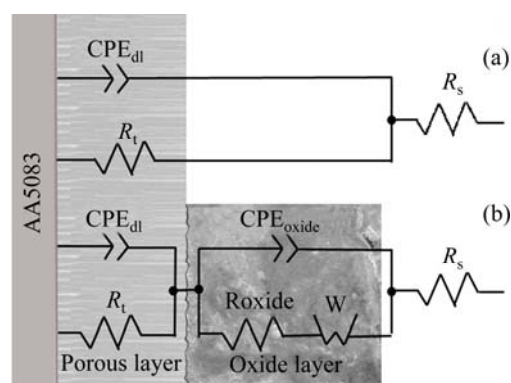


Fig. 6 Equivalent circuits for impedance spectra of IAA or AAA (a) and BAA (b) samples

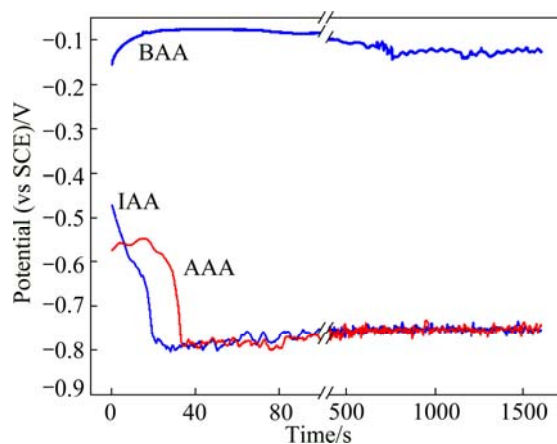
As shown in Fig. 6(b), the laterally complex hierarchical structure has a mixture of amorphous alumina and voids. For sample with BAA film, the diffusion process may become a control procedure in Faradaic processes. The behavior of Nyquist plot could be explained by a serial combination of diffusion CPE with a Warburg resistance (W). The compact intermediate layer has been demonstrated to replace the porous external surface and exhibits higher resistance.

Table 1 Equivalent circuits for impedance spectra of samples with IAA, AAA or BAA film

Sample	$R_s/$ ($\Omega \cdot \text{cm}^2$)	$R_f/$ ($\text{M}\Omega \cdot \text{cm}^2$)	CPE _{dl}		$R_{\text{oxide}}/$ ($\text{k}\Omega \cdot \text{cm}^2$)	CPE _{oxide}		Warburg		
			$T/$ ($\text{nF} \cdot \text{cm}^{-2}$)	n		$T/$ ($\text{nF} \cdot \text{cm}^{-2}$)	n	$R/$ ($\text{k}\Omega \cdot \text{cm}^2$)	$T/$ ($\text{nF} \cdot \text{cm}^{-2}$)	n
IAA	9.4	13.91	0.419	0.98	–	–	–	–	–	–
AAA	10.5	21.62	0.324	0.97	–	–	–	–	–	–
BAA	11.1	65.49	0.341	0.86	25.51	1.969	0.957	10.43	0.688	0.12

3.5 Corrosion behaviors at medium temperature

As shown in Fig. 7, the BAA sample presents a rather positive potential (–130 mV) with no sign of negative shift during 1500 s exposure, while the potentials of IAA film and AAA films were first started at –470 mV and –570 mV, respectively, and shifted rapidly to a rather negative potential (–750 mV) in 30 s. Similarly to IAA, the porous AAA film structure is dehydrated and the cell potential time transient has a comparable evolution, suggesting a similar oxide formation mechanism. It confirms with mechanism that the alternative accumulation through oxide film will affect the electric field of the surface and finally lead to a negative shift of the open circuit potential. Usually amorphous film layers are stable while the oxide on the film surface has a higher formation ratio than the inner oxide, which make it possible to reach a more positive surface.

**Fig. 7** Open circuit potential of IAA, AAA and BAA samples in 3.5% NaCl solution

Corrosion current densities (J_{corr}) of samples were calculated by means of the Tafel (Figs. 8(a), (b) and (c)) extrapolation method and the results are listed in Table 1. In addition, the results of the corrosion potentials (φ_{corr}), anodic and cathodic Tafel slopes (β_a , β_b) are presented in Table 2. The measured curves of samples are repeated three times and the results are accurate to 5%.

As observed in the polarization profiles, the increase of the testing temperature was accompanied by an increase in the corrosion current density associated with the active infiltration of chloride ions through the

outer surface of the film. The J_{corr} of the samples in 50 °C medium was limited about the quarter of that at 40 °C, while the φ_{corr} was affected significantly by a positive shift. The discrepancy for J_{corr} between unsealed sample and AAA sample may be explained by composition in porous structure which was dependent upon the sealing technique. Results of φ_{corr} for all samples, shift positively with the same order of $\varphi_{\text{corr-BAA}} > \varphi_{\text{corr-AAA}} > \varphi_{\text{corr-IAA}}$. Specifically, for all results in the range of 20–50 °C, the corrosion protection ability seemed to be effective with the lowest J_{corr} at 20 °C, while the noblest φ_{corr} was observed at 30 °C. The discrepancy for J_{corr} among IAA, AAA and BAA samples with the order of $J_{\text{corr-BAA}} < J_{\text{corr-AAA}} < J_{\text{corr-IAA}}$ may be explained by composition in porous structure which was dependent upon the sealing technique.

The rising temperature may accelerate the electron transfer and chloride ions transmission. Meanwhile, the specific adsorption of chloride ions will have an impact on autocatalytic generation of cation/oxygen pairs across the anodic graded layer. As a result, the anodic processes were accelerated and J_{corr} was increased hundredfold. However, the current density decreased at 50 °C, which may be a consequence of blocking in the top layer of the IAA and AAA films, and the following process was considered the validity of fractional motion.

4 Conclusions

1) The ionic equilibrium in micropores, accelerated by applied voltage and vibrating current during anodizing in boric–sulfuric–oxalic acid electrolyte, may boost the growth rate of porous structure. Around 70.1% formation efficiency of the resultant film was achieved.

2) Exterior pores are first dilated to 10–14 nm by voltage, and then longitudinally oriented to the thickness of ~9 μm . The positive influence of barrier type layer on corrosion behavior was proved by thermal sealing measurement, but at the same time the porous characteristic of the film was changed.

3) Pore layer after hydration, which performed hierarchical layer with tiny flakes, was found to restrict corrosion behavior at a rather low rate. All samples with AAO film exhibited stable protection at ambient temperature.

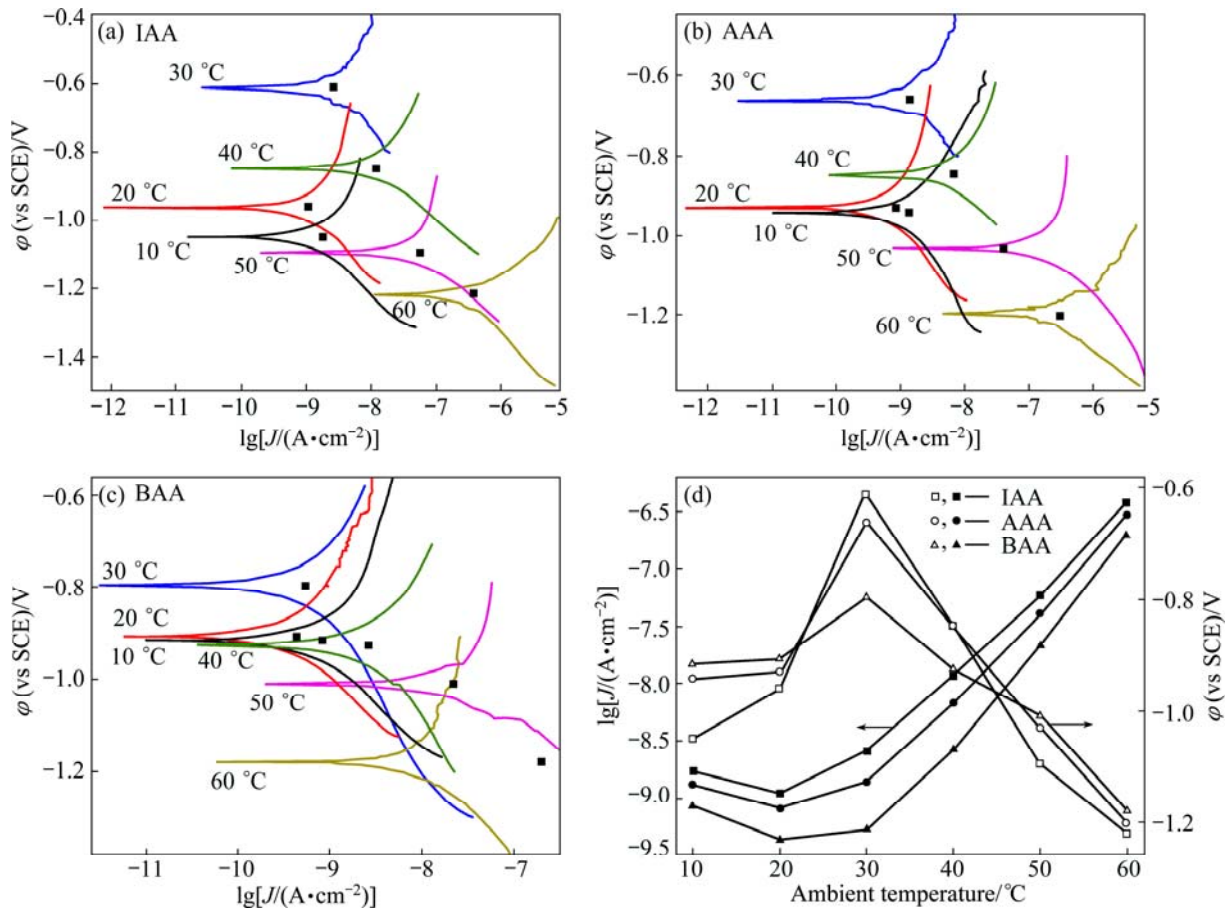


Fig. 8 Potentiodynamic curves (a, b, c) and self-corrosion behavior (d) of three experimental samples in 3.5% NaCl solution (10–60 °C)

Table 2 Potentiodynamic data of anodic film in 3.5% NaCl solution at different temperatures

Sample	Ambient temperature/°C	ϕ_{corr} (vs SCE)/V	J_{corr} ($\mu A \cdot cm^{-2}$)	β_a ($V \cdot dec^{-1}$)	β_b ($V \cdot dec^{-1}$)
IAA	10	-1.050	0.001742	0.276	0.176
	20	-0.960	0.001101	0.270	0.154
	30	-0.612	0.00261	0.308	0.211
	40	-0.847	0.01174	0.247	0.16
	50	-1.095	0.05885	0.444	0.149
	60	-1.220	0.3706	0.149	0.207
AAA	10	-0.942	0.001344	0.202	0.216
	20	-0.929	0.000826	0.300	0.197
	30	-0.662	0.001399	0.218	0.213
	40	-0.847	0.006741	0.262	0.153
	50	-1.032	0.04023	0.461	0.154
	60	-1.200	0.301	0.219	0.121
BAA	10	-0.915	0.00086	0.284	0.181
	20	-0.906	0.000441	0.267	0.183
	30	-0.795	0.000538	0.244	0.221
	40	-0.926	0.002658	0.221	0.208
	50	-1.010	0.02159	0.481	0.118
	60	-1.180	0.1995	0.513	0.183

References

- [1] HOUSER J E, HEBERT K R. The role of viscous flow of oxide in the growth of self-ordered porous anodic alumina films [J]. *Nature Materials*, 2009, 8: 415–420.
- [2] MA S J, LUO P, ZHOU H, FU C, KUANG Y, ZHANG R. Preparation of anodic films on 2024 aluminum alloy in boric acid-containing mixed electrolyte [J]. *Transactions of Nonferrous Metals Society of China*, 2008, 18(4): 825–830.
- [3] JAGMINAS A, ČEŠŪNIENĖ A, VRUBLEVSKY I, JASULAITIENĖ V, RAGALEVIČIUS R. Behavior of alumina barrier layer in the supporting electrolytes for deposition of nanowired materials [J]. *Electrochimica Acta*, 2010, 55(9): 3361–3367.
- [4] BERTHOLDO R, ASSIS M C, HAMMER P, PULCINELLI S H, SANTILLI C V. Controlled growth of anodic aluminum oxide films with hexagonal array of nanometer-sized pores filled with textured copper nanowires [J]. *Journal of the European Ceramic Society*, 2010, 30(2): 181–186.
- [5] VRUBLEVSKY I, JAGMINAS A, HEMELTJEN S, GOEDEL W A. Photoluminescent behavior of heat-treated porous alumina films formed in malonic acid [J]. *Applied Surface Science*, 2010, 256(7): 2013–2017.
- [6] OH J H, THOMPSON C V. The role of electric field in pore formation during aluminum anodization [J]. *Electrochimica Acta*, 2011, 56(11): 4044–4051.
- [7] THOMPSON G E, FURNEAUX R C, WOOD G C, RICHARDSON J A, GOODE J S. Nucleation and growth of porous anodic films on

- aluminum [J]. *Nature*, 1978, 272: 433–435.
- [8] LIU Jian-hua, LI Yong-xing, YU Mei, LI Song-mei, SUN Yu-jing. Effects of ammonium adipate on sulphuric acid anodizing of 7075-T6 aluminum alloy [J]. *Transactions of Nonferrous Metals Society of China*, 2012, 22(1): 324–330.
- [9] CURIONI M, KOROLEVA E V, SKELDON P, THOMPSON G E. Flow modulated ionic migration during porous oxide growth on aluminum [J]. *Electrochimica Acta*, 2010, 55(23): 7044–7049.
- [10] POTTS S E, SCHMALZ L, FENKER M. Ultra-thin aluminum oxide films deposited by plasma-enhanced atomic layer deposition for corrosion protection [J]. *J Electrochem Soc*, 2011, 158(5): C132–C138.
- [11] BARBOSA B, TAVARES S, COBUC A I, de MACÊDO M C S. Influence of microstructure on pitting corrosion resistance of alloy 904L superaustenitic stainless steel [J]. *Corrosion*, 2012, 68(8): 739–746.
- [12] SAEEDIKHANI M, JAVIDI M, YAZDANI A. Anodizing of 2024-T3 aluminum alloy in sulfuric–boric–phosphoric acids and its corrosion behavior [J]. *Transactions of Nonferrous Metals Society of China*, 2013, 23(9): 2551–2559.
- [13] DING G Q, YANG R, DING J N, YUAN N Y, SHEN W Z. Microscale steps and micro–nano combined structures by anodizing aluminum [J]. *Appl Surf Sci*, 2010, 256(21): 6279–6283.
- [14] MOON S, NAM Y, YANG C, JEONG Y. Growth of anodic oxide films on AC2A alloy in sulphuric acid solution [J]. *Corros Sci*, 2011, 53(4): 1547–1553.
- [15] YU K, HUANG Q, ZHAO J, DAI Y L. Electrochemical properties of magnesium alloy anodes discharged in seawater [J]. *Transactions of Nonferrous Metals Society of China*, 2012, 22(9): 2184–2190.
- [16] REN J J, YU Z. The anodizing behavior of aluminum in malonic acid solution and morphology of the anodic films [J]. *Applied Surface Science*, 2012, 261: 193–200.

非恒温电解液中 AA5083 Al–Mg 合金 阳极氧化膜的制备及其耐蚀性

王加余, 李澄, 郑顺利, 尹成勇, 王艳慧

南京航空航天大学 材料科学与技术学院, 南京 211106

摘要: 采用硼酸–硫酸–草酸电解液在铝合金表面制备有序多孔层, 研究阳极氧化过程中电流随时间的变化, 分析界面反应并计算膜层的生长效率。采用扫描电子显微镜、交流阻抗和动电位极化曲线研究膜层的微结构及其在不同温度环境下的耐蚀性。结果表明: 在氧化层界面双离子层浓度的增大有利于提高膜层的生长效率。所制备的阳极氧化膜厚度为 8~9 μm , 孔径为 10~14 nm, 膜层的微观形貌受金属基体组织结构的影响较大。在沸水封闭后膜层为分层结构, 表面呈细片状。氧化膜层封闭后能够明显降低试样的自腐蚀电流密度, 且耐蚀性随着环境温度的升高而具有更好的稳定性。

关键词: 5083 铝合金; 阳极氧化; 膜层生长效率; 腐蚀性能

(Edited by Xiang-qun LI)